Pellet studies with an upgrade fast camera system in the stellarator TJ-II

N. Panadero[1], D. Medina[2], K. J. McCarthy[1], G. Kocsis[3], T. Szepesi[3], I. García-Cortés[1], E. de la Cal[1], J. Hernández Sánchez[1], A. Ros[1], G. Motojima[4], TJ-II Team

[1] *Laboratorio Nacional de Fusión, CIEMAT, Madrid, Spain*
[2] *University Carlos III de Madrid, Leganés, Spain*
[3] *Centre for Energy Research, Budapest, Hungary*
[4] *National Institute for Fusion Science, Toki, Japan*

Plasma core fuelling is a key issue for the development of steady-state scenarios in magnetically confined plasma devices, particularly important for the helical types [1]. The primary candidate is cryogenic pellet injection (PI), which has been used for several decades [2]. However, a detailed understanding of some processes that occur during and after pellet ablation remains outstanding, in particular for non-axisymmetric devices. For such devices, the complexity of their magnetic fields, compared to tokamaks, make observations and analysis more intricate. With the aim of improving this situation, PI studies are carried out in the stellarator TJ-II with an upgrade fast-frame camera system. Such studies are focussed on pellet acceleration for different magnetic configurations. Moreover, experimental results are compared with the stellarator version of the HPI2 code, which has already been used for comparison with experimental data, without considering pellet acceleration, from TJ-II [3] and W7-X [4].

The TJ-II is a 4-period, low magnetic shear ($\Delta\iota \leq 6$ %) stellarator with a major radius R = 1.5 m, and an average minor radius $\langle a \rangle \leq 0.22$ m. Its magnetic-field is created by a set of copper coils, resulting in a bean shaped cross-section and central magnetic field, $B(0) \leq 1.1$ T. Plasmas are usually created and maintained using ECRH ($P \leq 500$ kW, $t \leq 300$ ms), achieving central electron densities, $n_e(0)$, of $\leq 1.7 \times 10^{19}$ m^{-3}, while electron and ion temperatures are $T_e(0) \leq 2$ keV and $T_i(0) \leq 120$ eV, respectively [5]. The TJ-II PI (see Figure 1) is a 4-barrel pipe gun device with a cryogenic refrigerator for *in-situ* pellet formation (10 K), fast propellant valves for pellet acceleration (v_p ~ 600-1200 m/s) and straight delivery lines. Cylindrical pellets, from 0.42 mm to 1 mm in diameter, contain between 3.1×10^{18} and 4.2×10^{19} H atoms. The PI is equipped with a light gate (LG) and a microwave cavity (MW) to estimate pellet velocity and mass [6]. Also, two amplified Si photodiodes, fitted with interference filters centred at 660 nm, follow the pellet cloud H_α emission (λ = 656.28 nm) from above (TOP) and behind (SIDE) pellet flight. In addition, a fast camera (FASTCAM APX-RS by Photron Inc.) records pellet injections from above (TOP) and tangential (TANG) to the flight path. It is equipped with a coherent fibre double bundle and a 12.5 mm lens. Its time resolution can be set from 1/frame rate to 1 μs, while the spatial resolution varies from 1024x1024 pixels to 16x128 pixels at maximum frame rate (250 kfps) (each pixel corresponds to ~0.6 mm to ~1 mm along the pellet flight path,

depending on the viewport). This system follows the pellet trajectory simultaneously from two different viewports, allowing for the 3D reconstruction of pellet trajectory.

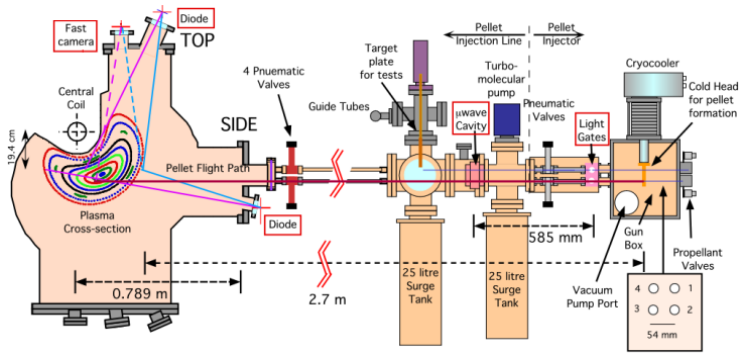

Figure 1. Cross-sectional sketch of the TJ-II vacuum chamber, magnetic surfaces, and the pellet injector. The relative locations of pellet Lines#1 through #4 are indicated with respect to the rear of the PI. [7]

In this study, pellet injections into ECRH plasmas and different magnetic configuration are analysed. As a representative example, discharge #51178 is presented, where a pellet was injected into the TJ-II standard configuration, 100_44_64. In Figure 2a) the H_α emission detected by the photodiode system is shown, together with the light profile from fast camera images. Moreover, in Figure 2b &c), montages of fast camera snap-shot images are presented.

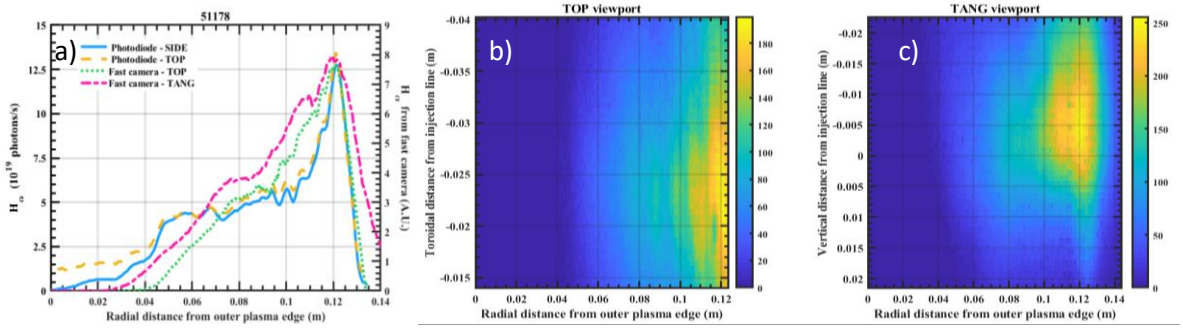

Figure 2. a) H_α emissions detected by the SIDE (solid blue) and TOP (dashed yellow) photodiodes, plus the light profile obtained from the fast camera (TOP – dotted green – and TANG – dash – dotted green), versus distance into plasma. They correspond to a pellet with 6.8x10^{18} H atoms injected into discharge #51178 at 952 m/s (calculated from the LG – MW system) along Line #1 into the TJ-II standard configuration. b and c) Montage of snap-shot images for discharge #51178 when a pellet with 6.8x10^{18} H atoms was injected along Line #1 at 952 m/s (frame rate is 87.5 kfps, exposure time is 1 μs) observed from b) TOP and c) TANG

From these fast camera images, pellet trajectories are reconstructed, and velocities and accelerations are estimated. For that, a simply quadratic fit is used (except for the toroidal position, which is assumed to remain constant). Results are shown in Figure 3.

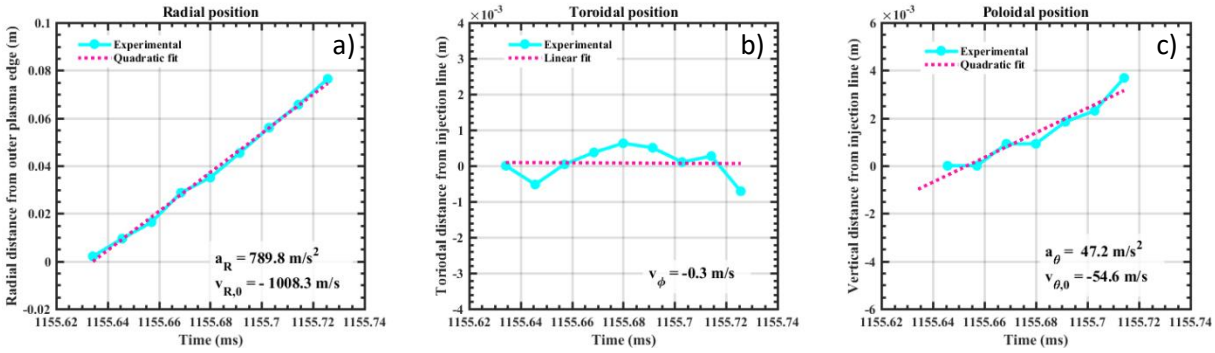

Figure 3. Pellet a) radial, b) toroidal and c) vertical positions (from fast-camera images) versus time after pellet entry into discharge #51178, along with accelerations and initial velocities obtained from data fits.

Same calculations are repeated for pellets injected into different configurations, namely 100_46_65, 100_48_64 and 100_50_65. Iota profiles for the standard configuration and 100_46_65 are found in Figure 4. The other two configurations follow the same tendency, *i.e.,* their iota profiles should be above 100_46_65. Results from the already mentioned analysis for these configurations are shown in Figure 5. Here, it can be observed that pellet radial acceleration seems to increase for configurations with higher iota, while the opposite appears to occur for the poloidal component.

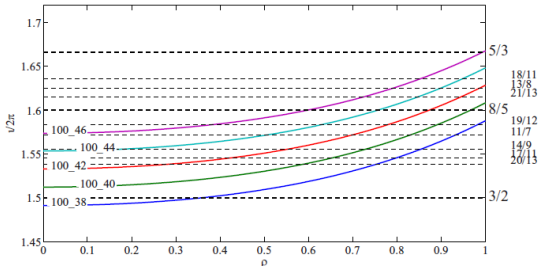

Figure 4. Iota profiles corresponding to different TJ-II magnetic configurations used during pellet injection experiments. Main rational surfaces are also indicated [8].

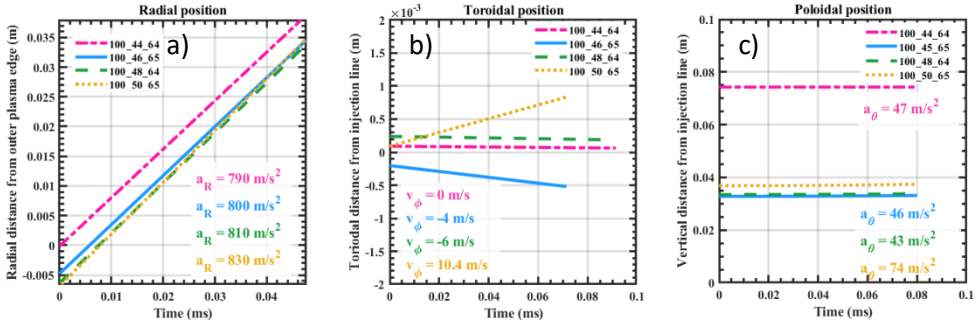

Figure 5. Pellet a) radial, b) toroidal and c) vertical positions (obtained from fast-camera images) versus time after pellet entry into different reproducible discharges of several TJ-II magnetic configurations (100_44_64 – dash-dotted magenta, 100_46_65 – solid blue, 100_48_64 – dashed green and 100_50_65 – dotted yellow). Estimated accelerations and initial velocities are also shown.

To complete the analysis, the HIP2 code [8–10] used here includes pellet acceleration in the simulation of ablation and deposition profiles. For that, the two models already included in the code [11] are extended to allow handling the vertical component of the acceleration. Predictions obtained with both models are compared with TJ-II experimental results, as observed in Figure 6, where the different predicted ablation profiles and pellet trajectories are found. It is observed

here that ablation profiles always reproduced the H_α profile, except for the intensity of the final peak. However, not all the collected light is attributed to the pellet cloud emission.

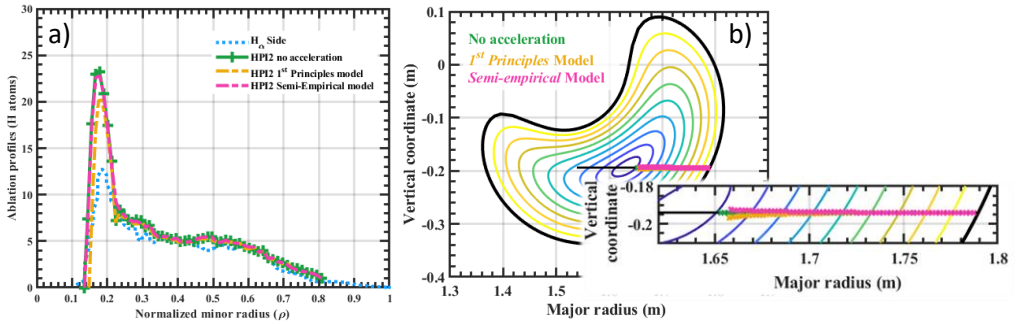

Figure 6. a) HPI2 ablation (solid green with crosses- no acceleration, dash-dotted yellow – 1st Principles model – and dash-dotted magenta – Semi-empirical model) profiles compared with measured Hα profile (dotted blue) for a pellet injected along Line #1 into #51178. b) Poloidal cross-sections corresponding to Line #1, indicated by a black line and a closed-up to the comparison of pellet trajectories for the three cases, i.e., with constant pellet velocity (green crosses); acceleration for the First Principles Model (yellow crosses) and acceleration for the Semi-Empirical model (magenta crosses).

Finally, pellet position obtained with these models are compared with results from fast camera images, as found in Figure 7. It is observed here that radial and toroidal accelerations are relatively well reproduced, while the vertical one is better reproduced by the Semiempirical model. However, its value is underestimated.

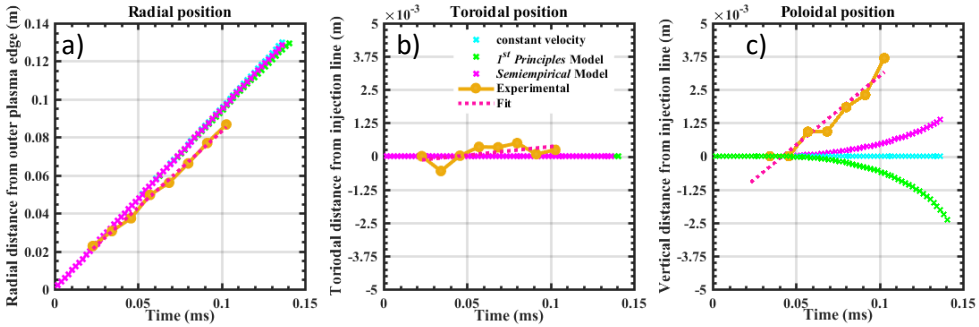

Figure 7. Pellet a) radial, b) toroidal and c) vertical positions estimated with HPI2 without pellet acceleration (cyan crosses), with the 1st Principles Model (green crosses) and the Semiempirical Model (magenta crosses) versus time after pellet entry into discharge #51178. In addition, data from fast camera from Figure 5 is also shown (experimental data in solid yellow with circles and fitting in dotted magenta).

"This work has been carried out within the framework of the EUROfusion Consortium and has received funding from the Euratom research and training programme 2014-2018 and 2019-2020 under grant agreement No 633053. The views and opinions expressed herein do not necessarily reflect those of the European Commission."

[1] H. Maaßberg, C.D. Beidler, E.E. Simmet, *Plasma Phys. Control. Fusion* **41** (1999) 1135–1153.
[2] B. Pégourié, *Plasma Phys. Control. Fusion* **49** (2007) R87.
[3] N. Panadero *et al.*, *Nucl. Fusion* **58** (2018) 026025.
[4] J. Baldzuhn *et al.*, *Plasma Phys. Control. Fusion* **61** (2019) 095012.
[5] E. Ascasíbar *et al.*, *Nucl. Fusion* **59** (2019) 112019.
[6] S.K. Combs *et al.*, *Fusion Sci. Technol.* **64** (2013) 513–520.
[7] K.J. McCarthy *et al.*, *Nucl. Fusion* **57** (2017) 056039.
[8] B.P. Van Milligen *et al.*, *Nucl. Fusion* **53** (2013) 93025–93032.
[9] B. Pégourié *et al.*, *Plasma Phys. Control. Fusion* **47** (2005) 17–35.
[10] B. Pegourie *et al.*, *Nucl. Fusion* **47** (2007) 44–56.
[11] F. Köchl *et al.*, *Prepr. EFDA–JET–PR(12)57* (2012) 82.
[12] T. Szepesi *et al.*, *J. Nucl. Mater.* **390–391** (2009) 507–510.